

X-ray and UV Orbital Phase Dependence in LMC X-3

Patricia T. Boyd ¹

Alan P. Smale ²

Laboratory for High Energy Astrophysics, Code 662, NASA/Goddard Space Flight Center, Greenbelt, MD 20771

Joseph F. Dolan

Laboratory for Astronomy and Solar Physics Code 681, NASA/Goddard Space Flight Center, Greenbelt, MD 20771

ABSTRACT

The black-hole binary LMC X-3 is known to be variable on time scales of days to years. We investigate X-ray and ultraviolet variability in the system as a function of the 1.7 day binary phase using a 6.4 day observation with the *Rossi X-ray Timing Explorer* (RXTE) from December 1998. An abrupt 14% flux decrease, lasting nearly an entire orbit, is followed by a return to previous flux levels. This behavior occurs twice, at nearly the same binary phase, but it is not present in consecutive orbits. When the X-ray flux is at lower intensity, a periodic amplitude modulation of 7% is evident in data folded modulo the orbital period. The higher intensity data show weaker correlation with phase. This is the first report of X-ray variability at the orbital period of LMC X-3. Archival RXTE observations of LMC X-3 during a high flux state in December 1996 show similar phase dependence. An ultraviolet light curve obtained with the *High Speed Photometer* aboard the *Hubble Space Telescope* shows orbital modulation consistent with that in the optical, caused by the ellipsoidal variation of the spatially deformed companion.

The X-ray spectrum of LMC X-3 can be acceptably represented by a phenomenological disk-black-body plus a power law. Changes in the spectrum of LMC X-3 during our observations are compatible with earlier observations during which variations in the 2-10 keV flux are tracked closely by the disk geometry spectral model parameter.

Subject headings: accretion, accretion disks — stars: individual (LMC X-3) — stars: black holes — stars: binaries: close — X-rays: stars

¹Also Joint Center for Astrophysics, University of Maryland Baltimore County

²Also Universities Space Research Association

1. Introduction

LMC X-3, a bright (up to 3×10^{38} erg s $^{-1}$) black hole candidate in the Large Magellanic Cloud, is a highly variable X-ray source. It exhibits at least two distinct emission states. During its more common high/soft state, the X-ray spectrum is similar to that of other high/soft state black hole candidates, with an "ultrasoft" component and a hard (>10 keV) tail. The low/hard state, on the other hand, is characterized by an X-ray spectrum described by a pure power law $I(E) = A_{pl}E^{-\Gamma}$ with $\Gamma \sim 1.8$ or less (Wilms et al. 2000), significant time variability with 30-50% modulation of the intensity, and a 0.4 Hz QPO (Boyd et al. 2000).

The B3 V optical counterpart of LMC X-3 (Warren and Penfold 1975) ($V \sim 16.7-17.5$) shows a large velocity range (semi-amplitude $K=235$ km s $^{-1}$) through its 1.7 day orbital period. The lack of eclipses indicates that the inclination of the system is $<70^\circ$, and this leads to a compact object mass of $\sim 7M_\odot$, making LMC X-3 a prime black hole candidate (Cowley et al. 1983, Paczynski 1983, Ebisawa et al. 1993, but see also Mazeh et al. 1986). The optical light curve shows minima at the times of conjunction of the two components, with amplitude ~ 0.2 mag each; the approximately equal minima of the optical light curve are consistent with an underlying ellipsoidal stellar surface (van der Klis et al. 1985). Comparing observations of the source over a long time baseline, it is apparent that the ratio of optical to X-ray flux is not constant. This may indicate secular variation of the disk structure over a time scale of a week, or a change in anisotropy of the X-ray emission (Treves et al. 1990).

The long-term X-ray luminosity of the system is strongly modulated on time scales of hundreds of days (Cowley et al. 1991, Wilms et al. 2000). The mean 2-10 keV X-ray flux varies by a factor of more than one hundred during this long-term cycle. This variability was previously attributed to the precession of a bright, tilted, and warped accretion disk. The discovery of recurrent low/hard states in LMC X-3 argues against this mechanism being responsible for the long term variation (Wilms et al. 2000).

Previous X-ray observations have detected no phase-related variability in LMC X-3, and the 1.7-day orbital period is not detected prominently in the RXTE ASM light curve. However, the Ginga and EXOSAT observations of this source were quite fragmentary –

seven observations with durations ranging from 1 to 24 ksec between December 1983 and December 1984 with EXOSAT (Treves et al. 1988), and a series of much shorter exposures spread over three years with Ginga (Cowley et al. 1991). Prior to the launch of RXTE, no intensive study of LMC X-3 sampling an entire binary cycle in a single epoch had ever been performed. We thus proposed an RXTE observation to create a large set of data covering several consecutive orbital cycles with the minimum of interruptions. We present here the results obtained from this observation, performed in 1998 December, along with a reanalysis of archival data from a shorter dedicated RXTE pointing two years earlier. We also include previously unpublished data from the High Speed Photometer aboard Hubble Space Telescope (HST), which is to our knowledge the only ultraviolet data on this source covering the 1.7 day binary orbit.

2. Observations

We observed LMC X-3 with RXTE (Bradt, Rothschild, & Swank, 1993) between 1998 December 08 17:17 UT – December 15 00:01 UT, for an on-source total good time of 283 kiloseconds. These observations are summarized in Table 1. The data presented here were obtained using the PCA instrument in the Standard 2 and Good Xenon data modes, with time resolutions of 16 sec and $< 1\mu$ sec respectively. The PCA consists of five Xe proportional counter units (PCUs), with a combined effective area of about 6500 cm 2 (Jahoda et al 1996). Only three of the five PCUs were on through the entire observation; we analyzed data only from these three detectors.

Spectra and light curves were extracted using the RXTE standard data analysis software, FTOOLS 5.0. PCA background subtraction was performed using the "L7-240" (v19990824/0909) faint source model. LMC X-3 is reliably detected above background out to about 18 keV. Response matrices were generated using PCARSP 2.43 in FTOOLS 5.0, with the latest energy-to-channel relationship. Spectral fitting was performed using XSPEC 11.0.

The optical counterpart of the X-ray source LMC X-3 was observed with the polarimetric detector of the High Speed Photometer (HSP) on the Hubble Space Telescope at six different orbital phases during the same binary orbit on 1993 August 24 12:09 UT – August 25 21:53 UT. The observations were obtained in the F277M bandpass using a 0.65 arcsec diameter

aperture. The FWHM response of the F277M filter to a flat incident spectrum is 2600 - 2940 Å. Further details on the instrumental characteristics of the HSP can be found in Bless et al. (1999).

The polarization in a source was determined from its count rate in four different analyzers, oriented at 0°, 45°, 90°, and 135°. Multiple measurements in each orientation analyzer were combined into a single set of count rates using the method recommended by Clarke et al. (1983). The normalized Stokes parameters and their associated uncertainties were then derived using the procedure outlined by Dolan et al. (1994). The magnitude of the polarization and its associated uncertainty were derived from the normalized Stokes parameters using the equations given by Dolan & Tapia (1986). The magnitude of polarization, p , was corrected for its non-normal distribution at low statistical significance (Simmons & Stewart 1985) using the correction factor of Wardle & Kronberg (1974).

Flux densities in the F277M bandpasses were calibrated by observations of BD +75° 325 (Bless et al. 1999), an O5p IUE spectrophotometric standard. To derive the flux density from the polarimetric observations, the count rates used were the average of the summed count rates in the 0° and 90° orientation analyzers and the summed count rates in the 45° and 135° pair (Dolan et al. 1994).

LMC X-3 was detected in our HSP observations during one orbital phase at the 80 σ level of significance in the count rate. The relatively larger uncertainties on the derived polarizations and the fluxes stated on an absolute scale are caused by photometric variations resulting from small differences in pointing after reacquisition of guide stars, coupled with the spherically aberrated images exceeding the diameter of the observing aperture (cf. Dolan et al 1994).

3. Time Variability

The long-term light curve of LMC X-3 as measured by the All-Sky Monitor (ASM) aboard RXTE is shown in Figure 1, where the four-day average count rate is plotted against Julian Date. The long term intensity variation is apparent, and clearly not strictly periodic. The vertical lines denote the epochs of the pointed PCA observations discussed in this paper. We first turn our attention to the later of these, which began on JD 2451155, at the moderately faint average ASM rate of ~ 1 count s^{-1} . Our RXTE PCA light curve of LMC X-3 is shown in Figure 2. The entire

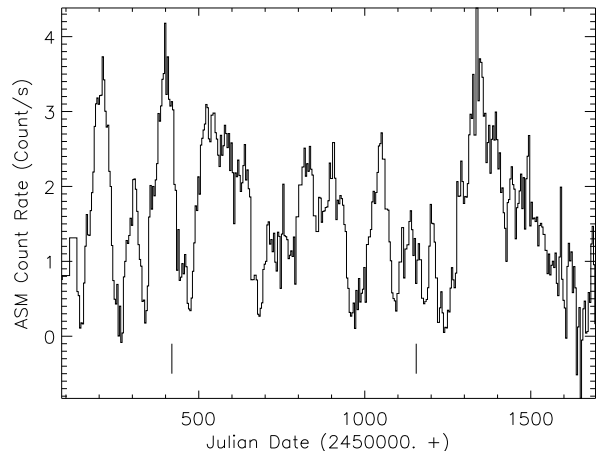


Fig. 1.— Long term variation of LMC X-3 as observed by the RXTE All-Sky Monitor. The four-day-average count rate is plotted against Julian Date. Not strictly periodic, the episodes have time scales from 64 days to 292 days. The PCA observations discussed in this paper are denoted with the short vertical lines at the bottom of the figure. The 1998 December observations occurred when the ASM rate was near the relatively low value of 1 count s^{-1} . An archival observation from 1996 December, when the ASM rate was near 3 count s^{-1} , is also discussed.

6.4 day coverage of our observing campaign is shown, along with 1- σ error bars. The PCA rate in counts s^{-1} is plotted against time in days (upper axis) as well as running binary phase (lower axis). Orbital phase is calculated using the van der Klis (1985) ephemeris, namely $T_0 = \text{HJD } 2445278.005 + 1.70479 * N$. Phase zero corresponds to superior conjunction of the X-ray source. The observations cover the ~ 3.5 consecutive binary orbits nearly uniformly, with only a few short gaps during this time.

3.1. Abrupt Flux Transitions

It is apparent in Figure 2 that there are two relatively flat stretches where the PCA rate stays near ~ 75 count s^{-1} for about one binary orbit, each of which abruptly ends with a flux decrease of $\sim 14\%$ to a rate of ~ 66 count s^{-1} . At each downward transition, the flux moves from the higher rate to the lower rate over a duration of ≤ 0.42 days. The one upward and two downward transitions occur at similar binary phases. The time at which the first down-

ward transition crosses the value of 70 count s^{-1} is $\sim \text{MJD } 51158.15$, phase 0.19. The time at which the upward transition crosses this level (on its return to the "nominal" flux level) is $\sim \text{MJD } 51159.85$, again binary phase 0.19—very nearly one integer binary orbit later. While the coverage gap immediately preceding the second downward transition makes the measured onset time uncertain (see Figure 2), we estimate it begins at or before $\sim \text{MJD } 51161.74$, phase ≤ 0.29 . In other words, the cycle from one downward transition to the next repeats at very nearly *twice* the orbital period. This is interesting, for it implies that the mechanism giving rise to the abrupt flux transitions is dynamically linked to the orbit.

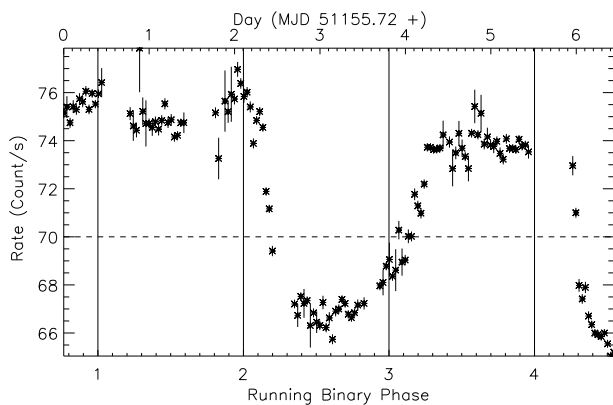


Fig. 2.— PCA light curve of LMC X-3 versus phase (lower X-axis) and time in MJD (upper X-axis) from 1998 December. The count rate is for a total of 3 PCUs. The time resolution is 3200 seconds. Vertical lines separate consecutive binary orbits. The horizontal dashed line represents our threshold for folding data at high and low flux (see text). An overall gross flux variation of $\sim 14\%$ is evident, with abrupt flux transitions recurring at \sim twice the orbital period of the binary. Less obvious at this scale is the sinusoidal *orbital* modulation, with an amplitude $\sim 5\%$.

3.2. Orbital Phase Dependence of X-ray Flux

We searched for evidence of X-ray modulation at the orbital period by dividing the data into two groups based on source counting rate. Data with a rate below 70 c/s were folded on the orbital period separately from those points with rate above 70 c/s , thus

preventing the gross flux transitions discussed above from contaminating the folded light curves. (Taking the data set as a whole and folding on the orbital period would result in data from higher and lower gross flux segments being averaged together in a single phase bin, which masks the lower-amplitude phase modulation.)

Figure 3 shows the results of folding each of these data sets on the orbital period of the van der Klis (1985) ephemeris. The orbital modulation is clear in the low-flux data (Fig. 3a)—it reaches a maximum slightly beyond $\phi = 0.0$ while the minimum occurs near $\phi = 0.5$. Folding the high-flux data (Fig. 3b) at the orbital period shows apparently weaker phase modulation.

To further investigate the presence of phase dependent flux variability, we performed periodogram analysis on the data set as a whole, binned at 800 s, and the phase-selected subsets defined above. We restricted the period search to within 0.5 days of the observed optical orbital period. Significance was estimated using the false-alarm probability defined by Scargle (1982). The best-fit trial period of the low-flux data is $1.693 \pm 0.037 \text{ d}$, with a false-alarm probability of 2.4×10^{-14} for a $> 7\sigma$ detection. The best-fit trial period for the high-flux data is $1.712 \pm 0.037 \text{ d}$, with false alarm probability of 4.5×10^{-11} for a $> 6\sigma$ detection. Each detection is significant and consistent with the observed orbital period in the optical. We conclude that significant periodic amplitude modulation is present in the X-ray flux from LMC X-3, and that the amplitude of the modulation is slightly higher when the 2-10 keV flux is lower. This is the first reported detection of orbital phase dependence in the X-ray intensity from LMC X-3.

3.3. Archival RXTE Observations during a high/soft state

Nowak et al. (2000) discuss a previous 140 ks RXTE observation of LMC X-3 obtained on 1996 November 30 – December 6, when the source was at the relatively high RXTE/ASM count rate of about 3.5 count s^{-1} . Their light curve (Figure 1 of Nowak et al. 2000) shows similar qualitative behavior: a slow flux transition from higher rate to lower rate in the 2-10 keV flux with an overall amplitude $\sim 12\%$. Motivated by the detection of strong phase dependence in LMC X-3 at relatively low flux levels, we extracted this archival data set to search for orbital modulation at a significantly different flux level and

epoch. Since different detectors were on/off through this observation, we scaled the lightcurve to the 5-pcu rate. Again, due to the overall gross flux transition present during this long observation, we grouped their data into two segments, selected by total PCA rate (above/below 410 count s^{-1}), before folding on the van der Klis (1985) ephemeris. The results of this analysis are presented in Figure 4. Phase dependence is clearly present in both groups of data. The phase coverage of the observation when the source was at slightly greater flux levels is insufficient to trace out an entire cycle; only orbital phase $\phi = 0.0\text{-}0.5$ was observed. At the lower count rate, the phase coverage is sufficient to trace out a light curve qualitatively similar to that seen in the low flux 1998 December data. As in the 1998 December observation, it is single-peaked; the maximum X-ray intensity occurs near $\phi = 0.95 - 0.05$ while the minimum is near $\phi = 0.5$. As in the 1998 December data, the amplitude of this modulation is $\sim 5\%$.

3.4. Searches for Rapid Time Variability

We searched for rapid aperiodic variability in LMC X-3 using the high time resolution PCA data obtained in the Good Xenon mode. Discrete power spectral density distributions (PSDs) were calculated by dividing the data into segments of uniform length, performing fast Fourier transforms of each, and averaging the results. The PSDs were normalized such that their integral gives the squared RMS fractional variability (Miyamoto et al 1991; van der Klis 1989). We subtracted the Poisson noise level from the power spectra, taking into account the modifications expected from PCA detector deadtime. In its low/hard state, LMC X-3 displays quasi-periodic oscillations (QPO) at a centroid frequency of 0.4 Hz, and significant time variability of 30–50% (Boyd et al. 2000). Neither are detected in this observation, and the long duration of this data set allows us to place a rather stringent upper limit of 1% on the rms amplitude of a QPO feature between 0.1–10 Hz.

3.5. Summary of Timing Results

Our analysis of the time variability in LMC X-3 indicates that the light curve shown in Figure 2 can be described as the superposition of 1) an orbital modulation of roughly constant amplitude and 2) abrupt flux transitions recurring at twice the orbital period. Significant orbital modulation is also present in archival data (Figure 4) taken when LMC

X-3 was at a dramatically different flux level, implying that orbital modulation is a reliable feature in the X-ray output through a fourfold range of source intensities. The 1996 December archival observation also contains one gross flux transition, though the data set is not long enough to determine whether it repeats, and if so, at what period. The amplitude of the orbital modulation in the 1996 December observation is approximately 5%, as in the 1998 December data.

4. HSP Results: UV Photometry and Polarimetry

Orbital modulation of the X-ray flux has not been previously observed in LMC X-3, although it is a well-known feature of the optical light curve. In the V-band, the ellipsoidal deformation of the B-star results in the double-peaked morphology of the light curve. In an effort to extend our knowledge of the orbital modulation of LMC X-3 as a function of photon energy, we present the results of an ultraviolet photometric and polarimetric study of LMC X-3 using the High Speed Photometer aboard the Hubble Space Telescope.

In Figure 5 we compare the orbital light curve we obtained in the F277M bandpass in 1993 with the V band light curve obtained in 1984 by van Paradijs et al. (1987). While the phase coverage of the UV light curve is sparse, the overall variation is not inconsistent with the double-peaked optical light curve. The UV light curve is also consistent with an additional source of UV radiation in the system, with maximum occurring near inferior conjunction of the X-ray source. This second light would presumably be coming from the accretion disk.

No linear polarization was detected at any orbital phase (see Table 2). Assuming constant polarization from LMC X-3 in the F277M bandpass, and treating the normalized Stokes parameters as normally distributed (but cf. Clarke et al. 1983), the 2σ upper limit on the linear polarization of LMC X-3 in the F277M bandpass is $p \leq 0.018$. Several other X-ray binary systems, notably Cygnus X-1, do show significant phase-dependent polarization in the UV, interpreted as evidence for single scattering off gas streams connecting the primary to the accretion disk (Dolan & Tapia 1988, Wolinski et al. 1996). The upper limit on any variable polarization is too large to contain any information about the structure of the gas streams in the system.

5. X-ray Spectral Variability

There is no single accepted model for the spectral variability of galactic black hole candidates across their several spectral states (see reviews by Tanaka & Lewin 1995, Nowak 1995, van der Klis 1995, for discussions of black hole spectral states). Numerous authors choose a phenomenological "disk black body plus power law" model, in which the spectrum is fit by the superposition of multiple rings of black bodies representing the cooler accretion disk, plus a power law to describe the hard photons. While not motivated by a clear physical picture of what gives rise to these independent components, this model does give reasonable results for spectral fits (though commonly a "feature" is seen at the cross-over point of the two functions). Alternative models based on a physical description of the interaction of a spherical Comptonizing corona and cooler seed photons from the disk (Shraeder & Titarchuk 1999, Borozdin et al., 1999) are often only applicable in restricted spectral states, or produce biased residuals at high energies. Because previous spectral studies of LMC X-3 have concentrated on the phenomenological "disk black body plus power law" model (Wilms et al. 2000, Nowak et al. 2000, also Ebisawa, Cowley), and because of the ambiguity in the spectral state of LMC X-3 at this relatively low flux level, we have chosen to report our spectral fitting results using this model. In the following discussion, model parameters for the power-law component are photon index Γ and A_{pl} in photons $\text{keV}^{-1} \text{cm}^{-2} \text{s}^{-1}$. The disk black body model is parameterized by T_{in} , the temperature (kT) at the inner edge of the accretion disk, as well as a geometric factor N which depends on the inner disk radius, the viewing angle of the accretion disk, and the distance to the source.

Wilms et al. (2000) report recurrent low/hard states in LMC X-3 based on long-term monitoring with RXTE over several years. This was confirmed by more recent RXTE observations during a low/hard state (Boyd et al. 2000) in which both the timing and spectral characteristics of black hole candidates in the low/hard state was observed. Wilms et al. (2000) report a disk temperature that drops below 1.0 keV as the source enters the low state. The source is well described by a pure power law with $\Gamma = 1.7$ when truly in the low state.

In our investigation of the spectral changes during our observation, we restrict ourselves to data obtained

far from SAA passage and with low measured electron contamination. We only consider observations where the orbital phase was between 0.475 to 0.525 in an attempt to minimize orbital effects when comparing the higher flux and lower flux spectra. Our spectral fits include data from 2.5-25.0 keV. The power law plus black-body disk model was found to be acceptable under the χ^2 test for each individual spectrum, with typical reduced χ^2 values near or below 1.0 for 49 degrees of freedom.

Results of spectral fits to the $\phi = 0.5$ observations are summarized in Table 3. A typical two-component model fit is shown in Figure 6. The disk temperature hovers near the critical value of $kT = 1.0$ reported by Wilms et al. (2000) as an indicator of the occurrence of a transition from the high/soft to the low/hard state. Unlike the pure low/hard state however, a significant disk component is required to achieve a reasonable spectral fit to the current observations. This may indicate that LMC X-3 was undergoing a state transition at the time. The model flux reported in Table 3 is about 15 times greater than the flux measured during the 2000 May low/hard state (Boyd et al. 2000).

The disk black body spectral components show a roughly linear trend with the 2-10 keV flux. The changes in T_{in} are small, and within the formal uncertainties on this parameter. On the other hand, the disk normalization parameter N varies by $\sim 20\%$ from minimum to maximum flux. Since N is proportional to $r_{in}^2 \cos\theta$ this implies either a change in the inner accretion disk radius, or the inclination of the disk, is responsible for the gross flux variation from one cycle to the next. A global warp or kink, traveling around the disk, could cause the effective inclination of the disk to vary from one binary cycle to the next.

Nowak et al. (2000) point out that, during the long observation in 1996 December, variations in the disk black body spectral components run counter to previously observed long term trends, wherein the normalization term remains fairly constant while the disk temperature exhibits marked variability with observed flux. Our results of the 1998 December observations follow the short time scale trend found by Nowak et al. (2000) where the disk black body temperature is relatively constrained and variability is instead correlated to the geometric normalization parameter.

6. Discussion and Conclusions

Our RXTE observations of LMC X-3 through 3.5 consecutive binary cycles have detected significant orbital phase modulation of the 2-10 keV X-ray flux. The amplitude of the orbital modulation is variable, being higher when the system experienced an abrupt decrease in flux. Comparison of our results to an archival observation at a profoundly different flux level shows that phase-dependent flux is a hallmark of LMC X-3 through a wide range of overall X-ray intensities, with an amplitude of between 5–10%. The UV light curve, while sparse, is consistent in shape with the optical variability, implying that the dominant component of the UV radiation is the deformed main sequence star and outer disk, as in the optical.

A phase-dependent X-ray flux may be due to a) a compact "hot spot" of X-ray generation moving into and out of our line of sight, b) a region of cooler absorbing matter moving into and out of our line of sight, or c) a combination of the two. Since LMC X-3 does not display eclipses of the compact object, its inclination is not well constrained. A possible geometric model that explains the variation seen at the different flux levels is that of a hot spot located between the main sequence star and the compact object, perhaps where the stream impacts the accretion disk. X-rays from this hot spot could be absorbed by the accretion disk at inferior conjunction of the X-ray source ($\phi = 0.5$) but be visible to the observer at superior conjunction ($\phi = 0$). The expected curvature of the gas stream would give rise to the flux maximum occurring slightly after superior conjunction. Changes in the location of the gas stream as a function of mass accretion rate could account for the slightly different phase of maximum during the high state 1996 observations.

An equally striking feature of our RXTE light curve is the abrupt flux decreases, separated by very nearly two binary periods. The slower return to the higher flux level also occurs near similar binary phase. One possible model for the system that explains both the overall flux transitions and the variable orbital phase modulation is that of a disk excited into a low-order global mode. Global instabilities in highly ionized accretion disks around compact objects are not sufficiently well understood to claim that this model is realistic or expected. However, there is growing numerical and observational evidence that suggests similar global structures in accretion disks do develop

and persist. Such a large-scale perturbation of the accretion disk provides a global mechanism for angular momentum transport and dispersion which, together with the local viscous processes, can drive the dynamics of the disk. Evidence for significant two-armed spiral structure has been seen in Doppler tomography studies of the dwarf nova IP Pegasi during two outbursts (Steeghs, 2000). Three dimensional hydrodynamical simulations of accretion disks show that the formation of spiral shocks is common over a wide range of system parameters, including disk temperatures much hotter than those in dwarf novae (Boffin et al. 1999). We suggest the presence of a global density wave in the accretion disk of LMC X-3 as one possible explanation that is consistent with the data. If such a global feature were stable for several binary orbits, and rotated with an angular velocity close to one quarter the orbital velocity, then the gross features in the X-ray light curve would be reproduced due to the varying obscuration along the line of sight. As the feature rotated around the disk it would at times obscure observed X-rays in a phase-dependent fashion, and at other times have little appreciable effect on the observed X-ray flux. This concept is illustrated schematically in Figure 7, where we represent the global mode as a spiral density wave. We do not rule out other combinations of disk- and orbital-geometry that may explain the observed behavior. We note, however, that the spiral structure seen in IP Peg, as well as large scale disc asymmetries in other systems, have been observed to co-rotate with the binary system.

The long term variability of LMC X-3 is not easily characterized. It is becoming clear that the previous conjecture of periodic large amplitude flux variations arising from a warped precessing disk is not complete: the large scale variation seen in the RXTE ASM (Figure 1) is far from simply periodic. If instead its long term behavior is similar to Cygnus X-1 and other persistent galactic black hole candidates, then LMC X-3 stands out due to the suggestion of a preferred time scale: on the order of hundreds of days from one low/hard state to the next. If a global disk instability is responsible for state transitions in such systems then the disk dynamics in LMC X-3 must be quite different from the persistent galactic black holes, which apparently undergo the transition in a more random fashion. It is possible that LMC X-3 does not fit neatly into either category above, but has characteristics of each. In that case, continued inten-

sive studies of the system should be carried out with the goal of developing a consistent physical model of the accretion disk structure and dynamics.

This research has made use of data obtained through the High Energy Astrophysics Science Archive Research Center Online Service, provided by NASA's Goddard Space Flight Center. ASM results were provided by the ASM/RXTE teams at MIT and at the RXTE SOF and GOF at NASA's GSFC. Based in part on observations with the Hubble Space Telescope obtained at the Space Telescope Science Institute, which is operated by AURA, Inc. under NASA contract NAS5-26555. We enjoyed helpful conversations with Mike Nowak and Joern Wilms. Karen Smale produced the artwork in Figure 7.

REFERENCES

- Bless, R. C., et al. 1999, *PASP*, 111, 364
- Boffin, M. J., Haraguchi, K. & Matsuda, T. 1999, "Disk Instabilities in Close Binaries—25 Years of the Disk-Instability Model," Mineshige S. & Wheeler J. C., eds, Universal Academy Press
- Borozdin, K., Revnivtsev, M., Trudolyubov, S., Shrader, C. R., & Titarchuk, L. G. 1999, *ApJ*, 517, 367
- Boyd, P. T., Smale, A. P., Homan, J., Jonker, P. G., van der Klis, M. & Kuulkers, E., 2000, *ApJ*, 542, L127
- Bradt, H. V., Rothschild, R. E., & Swank, J. H., 1993, *A&AS*, 97, 355
- Clarke, D., Stewart, B. G., Schwarz, H. E., & Brookes, A. 1983, *A & A*, 126, 260
- Cowley, A.P., Crampton, D., & Hutchings, J.B., 1983, *ApJ*, 272, 118
- Cowley, A. P., Schmidke, P. C., Ebisawa, K., Makino, F., Remillard, R. A., Crampton, D., Hutchings, J. B., Kitamoto, S. & Treves, A., 1991, *ApJ*, 381, 526
- Dolan, J. F., et al. 1994, *ApJ*, 432, 560
- Dolan, J. F., & Tapia, S. 1986, *PASP*, 98, 792
- Dolan, J. F., & Tapia, S. 1988, *Astron. Ap.*, v202, 124
- Ebisawa, K., Makino, F., Mitsuda, K., Belloni, T., Cowley, A. P., Schmidke, P. C. & Treves, A., 1993, *ApJ*, 403, 684
- Jahoda, K., Swank, J. H., Giles, A. B., Stark, M. J., Strohmayer, T., Zhang, W., & Morgan, E. H., 1996, in *EUV, X-ray and Gamma-Ray Instrumentation for Astronomy VII*, ed O. H. Siegmund (Bellingham, WA: SPIE), 59
- Mazeh, T., van Paradijs, J., van den Heuvel, E. P. J., Savonije, G. H., 1986, *A&A*, 157, 113
- Miyamoto, S., Kimura, K., Kitamoto, S., Dotani, T., & Ebisawa, K., 1991, *ApJ*, 383, 784
- Nowak, M. A., 1995, *PASP*, 107, 1207
- Nowak, M. A., Wilms, J., Heindl, W. A., Pottschmidt, K., Dove, J. B., & Begelman, M. C., 2000, *MNRAS*, in press (astro-ph/0005487)
- Paczynski, B., 1983, *ApJL*, 273, 81
- Scargle, J. D. 1982, *ApJ*, 263, 835
- Shrader, C. R., & Titarchuk, L. 1999, *ApJ*, 521, L121
- Simmons, J. F. L., & Stewart, B. G. 1985, *A&A*, 142, 100
- Steeghs, D., 2000, in preparation (astro-ph/0012353)
- Treves, A., Belloni, T., Chiappetti, L., Maraschi, L., Stella, L. et al., 1988, *ApJ*, 325, 119
- Treves, A., Belloni, T., Corbet, R. H. D., Ebisawa, K., Falomo, R. et al., 1990, *ApJ*, 364, 266
- Tanaka, Y., & Lewin, W. H. G., 1995, in *X-ray Binaries*, W. H. G. Lewin, J. van Paradijs, & E. P. J. van den Heuvel (eds.), Cambridge University Press, p. 126
- van der Klis, M., 1995, in *X-ray Binaries*, W. H. G. Lewin, J. van Paradijs, & E. P. J. van den Heuvel (eds.), Cambridge University Press, 252
- van der Klis, M., Clausen, J. V., Jensen, K., Tjemkes, J., van Paradijs, J. 1985, *A&A*, 151, 322
- van Paradijs, J., van der Klis, M., Augusteyn, T., Charles, P., Corbet, R. H. D. et al., 1987, *A&A*, 184, 201
- Wardle, J. F., & Kronberg, P. P. 1974, *ApJ*, 194, 249
- Warren, P. R., Penfold, J. E. 1975, *MNRAS*, 172, 41P
- Wilms, J., Nowak, M. A., Pottschmidt, K., Heindl, W. A., Dove, J. B., & Begelman, M. C., 2000, *MNRAS*, in press (astro-ph/0005489)
- Wolinski, K. G., Dolan, J. F., Boyd, P. T. et al. 1996, *ApJ*, 457, 759

This 2-column preprint was prepared with the AAS L^AT_EX macros v4.0.

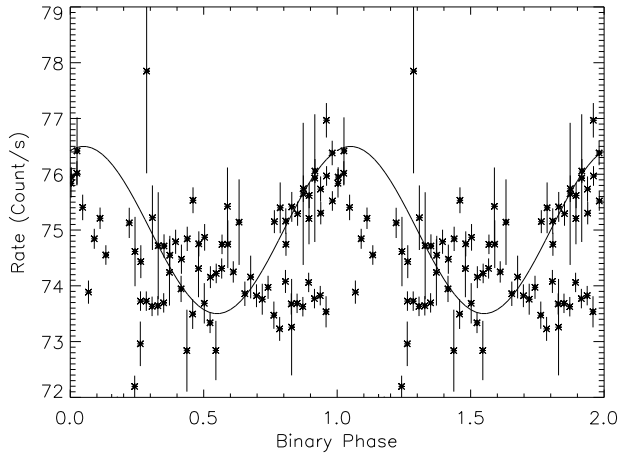
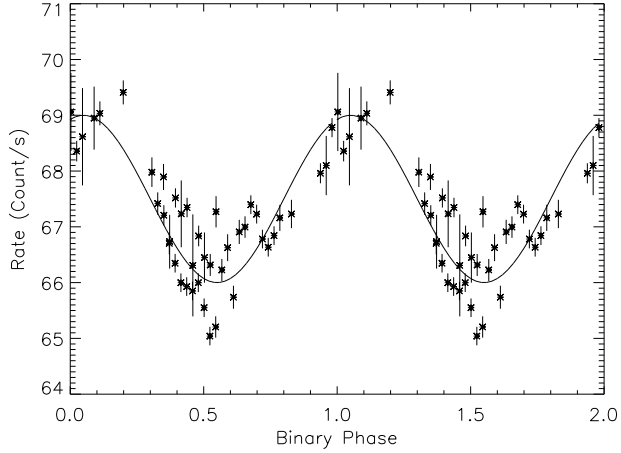


Fig. 3.— The PCA light curve from the 1998 December observations, folded on the 1.7 day binary period. The top panel includes only data where the rate is $< 70 \text{ count s}^{-1}$; at these lower fluxes, the amplitude of the orbital variation is 7%. The lower panel shows the folded higher-flux data ($> 70 \text{ count s}^{-1}$). Phase variability at this count rate is less significant. A sine wave with the same period and phase has been superimposed on each plot to guide the eye.

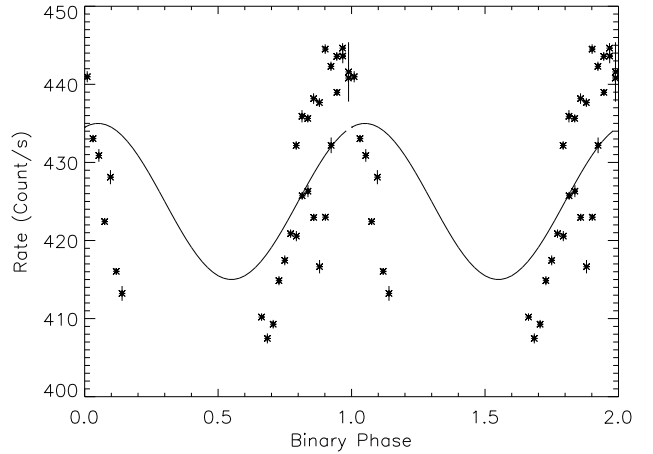
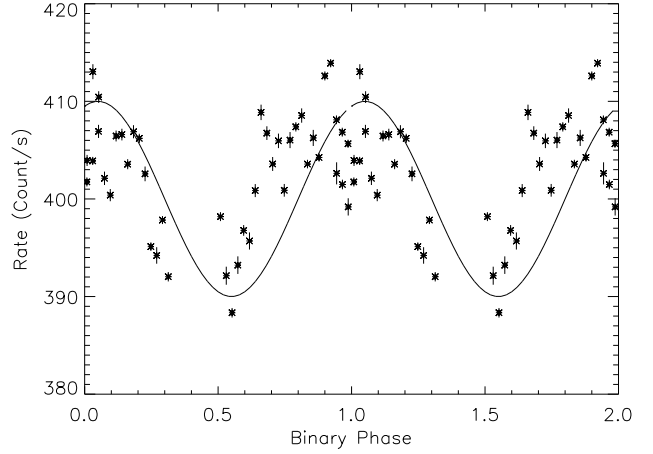


Fig. 4.— Archival PCA observation of LMC X-3 from 1996 December, folded on binary phase. Rate is for 5 PCUs. (See Nowak et al. 2000, Figure 1, for discussion.) Top panel: data below 410 count s^{-1} . Bottom panel: data above 3.5 count s^{-1} . The ASM rate during this observation was about 3.5 count s^{-1} . The phase-folded data show a light curve shape similar to the 1998 December observation, when the ASM rate was 1 count s^{-1} . A sine wave with the same phase and period as shown in the previous figure has been superimposed on both panels to guide the eye.

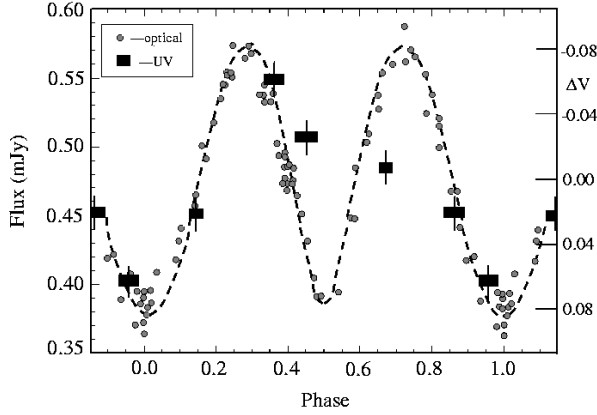


Fig. 5.— The UV lightcurve from HST obtained in 1993 (this paper, rectangles) superimposed on the optical V lightcurve from 1984 (van Paradijs, 1987, circles). UV flux is given on the left hand axis; V-band magnitude on the right hand axis. The two scales are independent; their intervals were adjusted to give the same amplitude in each band pass. While its phase coverage is sparse, the UV variability is consistent with the optical light curve.

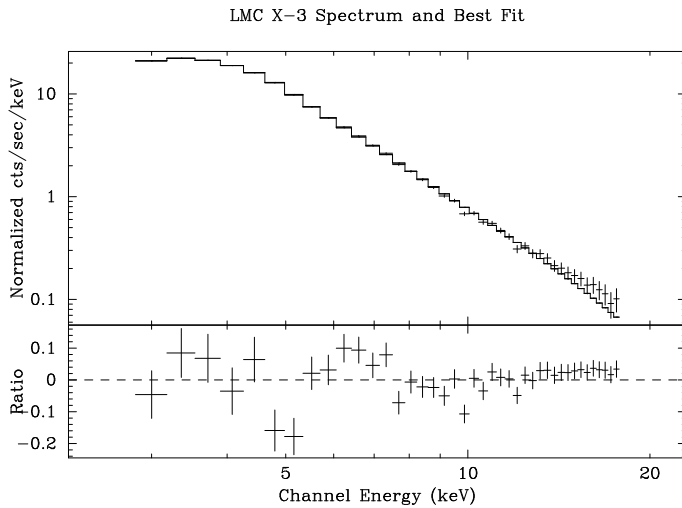


Fig. 6.— PCA spectrum of LMC X-3 and best-fit disk black body plus power law model for observation 24 (in Table 1). The ratio of the model to the data is shown in the lower panel. Parameters of the fit are listed in Table 3.

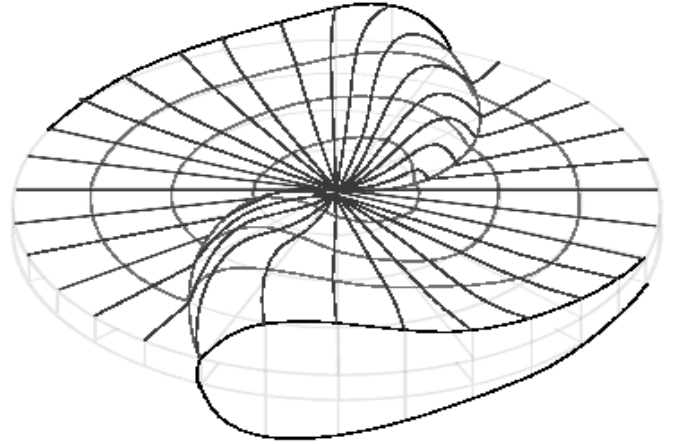


Fig. 7.— A schematic representation of a low order global oscillation mode excited in an accretion disk. If such a feature were stable for several binary orbits, and rotated with an angular velocity close to one quarter the orbital velocity, then the gross features in the X-ray light curve would be reproduced due to the varying obscuration along the line of sight.

TABLE 1
LMC X-3 RXTE OBSERVATION LOG, 1998 DEC 8 - 15

Obs	Start MJD	Exp Time (s)	Orbital Phase	Rate (count s ⁻¹)
1	51155.719	17032.0	0.765	74.30
2	51156.042	10592.0	0.955	75.77
3	51156.516	2762.0	0.232	74.36
4	51156.633	1216.0	0.301	75.89
5	51156.700	14248.0	0.340	74.95
6	51156.993	11208.0	0.512	74.10
7	51157.512	1920.0	0.816	75.04
8	51157.633	1368.0	0.887	76.71
9	51157.701	16404.0	0.929	76.18
10	51158.000	15355.0	0.103	74.01
11	51158.422	12740.0	0.350	68.18
12	51158.710	14058.0	0.520	67.62
13	51158.970	18031.0	0.671	67.89
14	51159.242	1340.0	0.831	69.08
15	51159.421	11099.0	0.937	69.47
16	51159.710	14266.0	0.106	71.14
17	51159.969	16895.0	0.258	74.25
18	51160.241	1664.0	0.418	75.51
19	51160.309	1536.0	0.457	76.03
20	51160.381	14087.0	0.500	74.86
21	51160.710	14749.0	0.693	73.89
22	51160.967	17920.0	0.844	74.36
23	51161.709	22855.0	0.280	67.89
24	51162.042	12544.0	0.474	66.54

TABLE 2
UV PHOTOMETRY AND POLARIMETRY OF LMC X-3, 1993 AUGUST 24 - 25

Orbital Phase	Flux (mJy)	Polarization
0.655 - 0.687	0.485 ± 0.012	0.016 ± 0.018
0.835 - 0.891	0.452 ± 0.012	0.014 ± 0.024
0.934 - 0.981	0.402 ± 0.011	0.000 ± 0.030
0.127 - 0.161	0.451 ± 0.012	0.000 ± 0.022
0.334 - 0.389	0.549 ± 0.013	0.000 ± 0.021
0.423 - 0.480	0.506 ± 0.012	0.017 ± 0.017

TABLE 3
PARAMETERS OF $\phi = 0.5$ SPECTRAL FITS

$L_x \times 10^{37} \text{ erg s}^{-1}$	Orbital Phase	Γ	A_{pl}	T_{in} (keV)	N	Obs
10.96	0.512	$3.24^{+0.06}_{-0.40}$	$0.16^{+0.021}_{-0.103}$	$1.01^{+0.010}_{-0.004}$	$27.5^{+2.60}_{-0.50}$	6
10.72	0.500	$2.83^{+0.01}_{-0.16}$	$0.087^{+0.01}_{-0.015}$	$1.02^{+0.001}_{-0.013}$	$27.2^{+0.50}_{-0.50}$	20
9.63	0.52	$3.03^{+0.07}_{-0.13}$	$0.21^{+0.039}_{-0.056}$	$0.98^{+0.008}_{-0.012}$	$21.9^{+2.00}_{-1.90}$	12
9.39	0.474	$3.08^{+0.07}_{-0.13}$	$0.21^{+0.069}_{-0.053}$	$0.954^{+0.015}_{-0.002}$	$23.9^{+1.50}_{-1.10}$	24